Preprints, 10th IFAC International Symposium on
Advances in Automotive Control
Columbus, Ohio, USA, August 28-30, 2022

Two Layer Model Reference Adaptive Control based on State Feedback for Engine Slipping Start of Parallel Hybrid Electric Vehicles

Cheng Peng, Li Chen*

** State Key Laboratory of Ocean Engineering of Shanghai Jiao tong University, Shanghai, 200240, China (email: li.h.chen@sjtu.edu.cn).*

Abstract: During engine slipping start (ESS) of parallel hybrid electric vehicles (HEV) with a dual-clutch transmission, the motor needs to propel the vehicle and crank the engine via the slipping clutch simultaneously. However, a lack of capability to respond to changes in driver demand can disturb normal driving habits. Meanwhile, parametric uncertainty of the clutch friction coefficient makes it hard to compensate for the clutch slipping torque. To guarantee response speed to changes in driver demand torque, a two-layer model reference adaptive controller (MRAC) is proposed for ESS utilizing state varialbes as the feedback. Under this framework, appropriate reference profiles can be generated according to the real-time driver demand torque rather than assuming that the accelerator pedal is unchanged. An auxiliary reference model is introduced in addition to the major reference model to modify the convergence rate of the tracking error without changing the well-designed reference profiles, and adaptive control laws are accordingly developed to enhance the transient performance against matched parameter uncertainty of clutch and unmatched measurement noise.

Keywords: Engine slipping start, hybrid electric vehicle, two-layer model reference adaptive control, transient performance, riding comfort

1. INTRODUCTION

With the increasing demand for energy efficiency and emission, hybrid electric vehicles (HEVs) have gained worldwide popularity due to their enhancements on energy-saving and low-emission while meeting the mileage requirements (Biswas *et al.*, 2021). Among different configurations, the parallel HEV with a dual-clutch transmission (DCT), which benefits from shifting without power interruption, has attracted extensive interest in the automotive industry (Kim and Choi, 2020). As seen in Fig. 1, the configuration allows the driving motor to crank the engine quickly by large torque transmitted through the slipping clutches, so that the traditional engine starter can be removed. However, the cranking operation, which is also called engine slipping start (ESS), is usually required when the HEV is running, for example, during the mode transition from the motor driving (MD) mode to combined driving (CD) mode, which is so-called engine slipping start (ESS). The torque and speed profile during this process are described in Fig. 2. Since the motor is connected to the output shaft directly, unexpected vehicle jerk and sluggish response speed to the changes in driver demand can be caused by the unreasonable distribution of motor torque, then, both the riding comfort and vehicle drivability has been deteriorated. Hence, a control strategy for ESS should be designed to guarantee the riding comfort and the response speed to changes in driver demand torque.

Most of the existing studies on the ESS issue focused merely on the riding comfort but neglected the possibility that driver changes the accelerator pedal just during this process. Constant vehicle speed or acceleration are generally chosen as the reference input for the design of the ESS controller. Mu-

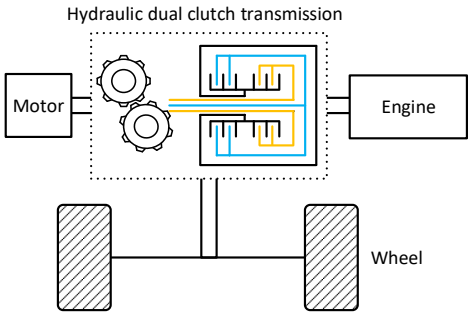

Fig. 1 Configuration of a parallel HEV equipped with a DCT.

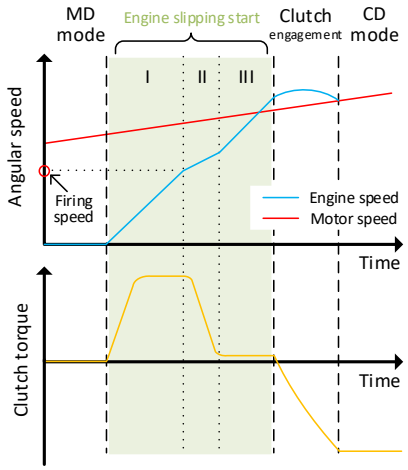

Fig. 2 ESS in the mode transition from MD mode to CD mode.

synthesis robust control and feedforward-linear quadratic regulator feedback technology were developed to improve the

tracking accuracy against system uncertainties in (Zhang *et al.*, 2016) and (Du *et al.*, 2017), respectively. To reduce the vehicle jerk, linear quadratic regulator-based closed-loop control was adopted in (Zhou *et al.*, 2020). However, with such reference profiles, the motor would not respond to the changes of the driver demand torque during the ESS. The normal driving habits are disturbed, leading to deterioration in drivability and resulting in potential safety hazards.

On the other hand, instead of tackling the ESS as a tracking problem, some studies use the sum of driver demand torque and clutch slipping torque as the motor torque demand directly (Yang *et al.*, 2020; Cong *et al.*, 2021). However, the parametric uncertainties of the clutch friction coefficient make it hard to obtain accurate clutch slipping torque.

In this paper, a two-layer MRAC with transient performance enhancement is proposed based on state feedback to guarantee the riding comfort and response speed to changes in driver demand torque of ESS. Different from the classical MRAC (Peng *et al.*, 2018), by introducing an auxiliary reference model, the two-layer MRAC can increase the convergence rate of tracking error between the plant and the major reference model without changing the desired dynamics of the major reference model (Anderson *et al.*, 2021). Taking the dynamics of the output shaft as the major reference model, an appropriate reference speed profile generated according to the driver demand torque can be obtained in real-time. Considering the parametric uncertainty of clutch friction coefficient and unmodeled uncertainties, i.e., measurement noise, adaptive control laws for the motor torque are generated. The transient performance with high adaptive gains is enhanced. The effectiveness of the designed controller is verified by simulation.

This paper is organized as follows. Section 2 builds mathematical models for the driveline. Section 3 derives the control law of the two-layer MRAC. Section 4 provides the simulation results. Conclusions are drawn in section 5.

2. DRIVELINE MODELING

As seen in Fig. 1, the driveline of HEV with DCT is composed of an engine, a motor, and a six-speed hydraulic DCT.

2.1 Driveline model of HEV with DCT

The simplified model is established in Fig. 3 for ease of analysis on driveline dynamics. As seen in Fig. 3, J_e, J_{tm}, J_v are the inertia moment of engine, motor, and vehicle body, respectively; T_e, T_{tm}, $T_{c,1}$, $T_{c,2}$, and T_r are the engine output torque, motor output torque, and clutch transmitted torque of clutch 1 and clutch 2, and the vehicle load torque, respectively; ω_e, ω_{tm}, and ω_w are the angular speed of the clutch disks of the engine side and motor side, and wheels, respectively; k_s and b_s are the spring stiffness and damping coefficient of the output shaft; b_e and b_{tm} are the damping coefficients of the engine and motor, respectively; $i_{t,1}$, $i_{t,2}$, and i_f are the gear ratio of transfer shaft 1, shaft 2 of DCT, and final reduction, respectively.

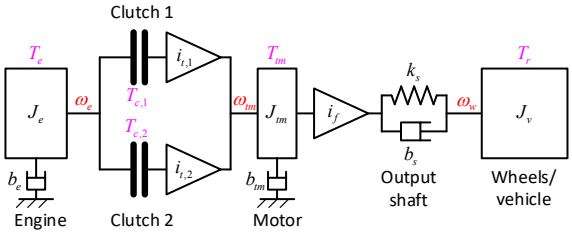

Fig. 3 Simplified driveline model of HEV with DCT.

It is noted that both of the shifting clutches can be assisted to drag the crankshaft, but in a single ESS, only one of them is actuated, while the other one is open. For unified description, the transmitted clutch torque is represented by T_c instead of $T_{c,1}$ and $T_{c,2}$ no matter the working clutch is clutch 1 or clutch 2. Similarly, the relative gear ratio is represented by i_t instead of $i_{t,1}$ and $i_{t,2}$. Therefore, universal governing equations are derived to describe the dynamics of the HEV driveline as

$$J_e\dot{\omega}_e(t) = T_e(t) + T_c(t) - b_e\omega_e(t), \tag{1}$$

$$J_{tm}\dot{\omega}_{tm}(t) = T_{tm}(t) - T_c(t) - \frac{1}{i_t i_f}T_s(t) - b_{tm}\omega_{tm}(t), \tag{2}$$

$$J_v\dot{\omega}_w(t) = T_s(t) - T_r(t) \tag{3}$$

where T_s is the shaft torque of the driveline expressed as

$$T_s(t) = k_s\left(\frac{1}{i_t i_f}\theta_{tm}(t) - \theta_w(t)\right) + b_s\left(\frac{1}{i_t i_f}\omega_{tm}(t) - \omega_w(t)\right), \tag{4}$$

θ_{tm} and θ_w are angular displacement of motor and wheels.

The vehicle load torque T_r is composed of the wind, gravity, and rolling resistance (Chen *et al.*, 2012), which can be expressed as

$$T_r = R\left(\frac{1}{2}c_D A_V \rho_{air} v^2 + mg\sin\alpha_r + f\cdot mg\cos\alpha_r\right) \tag{5}$$

where c_D is the aerodynamic drag coefficient, A_V is the vehicle frontal area, ρ_{air} is the air density, v is the vehicle speed, α is the road inclination angle, m is the vehicle mass, f is the rolling resistance coefficient, and R is the tire radius.

To better describe the process of ESS, it is divided into three phases, i.e., engine cranking phase, clutch disengaging phase, and engine firing and accelerating phase, as seen in Fig. 2.

2.2 Modelling of torque actuation components

2.2.1 Engine and motor output torque modeling

Considering the response delay, the engine output torque after ignition can be modeled by a first-order lag module empirically as

$$T_e(t) = \frac{1}{\tau_e\cdot s + 1}T_e^*(t) \tag{6}$$

where T_e^* is the torque command of the engine, τ_e is the time constant of the first-order transfer function of the engine.

Considering the rapid response and high accuracy, the output torque of the motor is modeled without time delay as

$$T_{tm}(t) = T_{tm}^*(t) \tag{7}$$

where T_{tm}^* is the torque command of the motor.

2.2.2 Clutch transmitted torque modeling

The clutch slipping torque T_c is expressed according to the Coulomb friction model as

$$T_c(t) = \mu_c \Delta P_c(t) A_c N_c R_c \cdot \mathrm{sgn}(\omega_{tm} - \omega_e) \tag{8}$$

where μ_c is the friction coefficient of the clutch disk, ΔP_c is the effective pressure on the clutch disks, N_c is the number of clutch surface, and R_c is the effective radius of clutch disk. The sign function $\mathrm{sgn}(\cdot)$ is defined as $\mathrm{sgn}(x) = \begin{cases} +1 & x > 0 \\ -1 & x < 0 \end{cases}$.

2.3 State-space system representation

Since the engine is disengaged from the driveline during ESS, the dynamics of the output shaft are determined by motor torque and clutch slipping torque. By denoting system state variables as $x = [\omega_{tm}, \omega_w, T_s]^T$, control input as $u = T_{tm} - T_c$, and disturbance input as $u_d = T_r$, the state-space representation of dynamics of the output shaft is derived according to (1) and (2) for controller design as

$$\dot{x}(t) = Ax(t) + Bu(t) + B_d u_d(t) \tag{9}$$

where

$$A = \begin{bmatrix} -\frac{b_{tm}}{J_{tm}} & 0 & -\frac{1}{J_{tm} i_t i_f} \\ 0 & 0 & \frac{1}{J_v} \\ \frac{k_s}{i_t i_f} - \frac{b_{tm} b_s}{J_{tm} i_t i_f} & -k_s & -\frac{b_s}{J_{tm}(i_t i_f)^2} - \frac{b_s}{J_v i_t i_f} \end{bmatrix}, \tag{10}$$

$$B = \left[\frac{1}{J_{tm}} \quad 0 \quad \frac{b_s}{J_{tm} i_t i_f}\right]^T, B_d = \left[0 \quad -\frac{1}{J_v} \quad -\frac{b_s}{J_v}\right]^T.$$

3. CONTROL STRATEGY DESIGN

The scheme of the proposed two-layer MRAC based on state feedback is presented in Fig. 4. By introducing an auxiliary reference model, the adjustable mechanism tunes the adaptive feedback control law according to the tracking error of state variables between the control plant and the major reference model together with deviation between the tracking error and state variables of the auxiliary reference model.

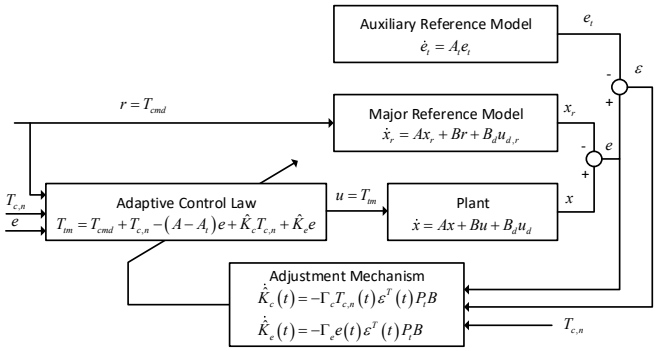

Fig. 4 Scheme of two-layer MRAC based on state feedback

3.1 Reference model

3.1.1 Major reference model

Since the vehicle is in MD mode before the ESS, the driveline dynamics during MD mode is selected for the development of the major reference model, so that the driveline dynamics of ESS can behave as that of the MD mode and the driving sense can be kept. By choosing the reference signals as $x_r = [\omega_{tm,r}, \omega_{w,r}, T_{s,r}]^T$, reference input as $r = T_{cmd}$, and disturbance input as $u_d = T_r$, the reference model can be written as

$$\dot{x}_r(t) = Ax_r(t) + Br(t) + B_d u_{d,r}(t) \tag{11}$$

where T_{cmd} is the driver demand torque,

$$A = \begin{bmatrix} -\frac{b_{tm}}{J_{tm}} & 0 & -\frac{1}{J_{tm} i_t i_f} \\ 0 & 0 & \frac{1}{J_v} \\ \frac{k_s}{i_t i_f} - \frac{b_{tm} b_s}{J_{tm} i_t i_f} & -k_s & -\frac{b_s}{J_{tm}(i_t i_f)^2} - \frac{b_s}{J_v i_t i_f} \end{bmatrix}, \tag{12}$$

$$B = \left[\frac{1}{J_{tm}} \quad 0 \quad \frac{b_s}{J_{tm} i_t i_f}\right]^T, B_d = \left[0 \quad -\frac{1}{J_v} \quad -\frac{b_s}{J_v}\right]^T.$$

3.1.2 Auxiliary reference model

An auxiliary reference model is introduced to the MRAC system in addition to the major reference model. As the convergence of the tracking error with respect to the reference model is subject to the properties of A, which is defined by vehicle parameters, the auxiliary reference model can modify the behavior of the tracking trajectory and enhance the transient performance. Denoting trajectory as e_t, the auxiliary reference model that predefines the tracking error's transient dynamics is obtained as

$$\dot{e}_t(t) = A_t e_t(t) \tag{13}$$

where A_t is Hurwitz, and $\mathrm{Re}(\lambda_{\max}(A_t)) < \mathrm{Re}(\lambda_{\min}(A))$.

3.2 Error dynamics

To design a torque control to make the driveline dynamics (9) behave like the reference model (11), define the model-following error as

$$e(t) = x(t) - x_r(t) . \tag{14}$$

Assuming that the nominal vehicle resistance torque is reliable, using (9) and (11) yields

$$\dot{e}(t) = Ae(t) + B\left(T_{tm}(t) - T_{cmd}(t) - T_c(t)\right). \tag{15}$$

Considering the auxiliary reference model, the deviation ε of tracking error e with respect to e_t is defined as

$$\varepsilon(t) = e(t) - e_t(t). \tag{16}$$

Therefore, the dynamics of ε is derived according to (13), (15), and (16) as

$$\dot{\varepsilon}(t) = A_t\varepsilon(t) + (A - A_t)e(t) + B\left(T_{tm}(t) - T_{cmd}(t) - T_c(t)\right). \tag{17}$$

3.3 Adaptive control law development

Considering the parametric uncertainty of clutch friction coefficient, the control law of motor torque T_{tm} is designed as

$$T_{tm}(t) = T_{cmd}(t) + (1 + K_c)T_{c,n}(t) + K_{e,n}e(t) + K_e e(t) \tag{18}$$

where $T_{c,n}(t)$ is nominal clutch slipping torque, K_c is the unknown part of clutch friction coefficient, $K_{e,n}$ and K_e are the known part and unknown part of feedback gain of $e(t)$, respectively. Wherein there exists $A_t = A + BK_{e,n}^T$.

Since feedback gains K_c and K_e are unknown, the adaptive law for $\hat{K}_c$ and $\hat{K}_e$ are given as

$$\dot{\hat{K}}_c(t) = -\Gamma_c T_{c,n}(t)\varepsilon^T(t)P_t B , \tag{19}$$

$$\dot{\hat{K}}_e(t) = -\Gamma_e e(t)\varepsilon^T(t)P_t B \tag{20}$$

where Γ_c and Γ_e are positive adaptive learning gains, P_t is the symmetric, positive-definite solution of the algebraic Lyapunov equation

$$0 = A_t^T P_t + P_t A_t + Q_t \tag{21}$$

and Q_t is also symmetric and positive-definite.

3.4 Stability analysis

To prove the stability of the proposed two-layer MRAC, consider the Lyapunov function candidate as

$$V\left(t, \varepsilon, \hat{K}_c, \hat{K}_e\right) = \varepsilon^T P_t \varepsilon + \mathrm{tr}\left(\tilde{K}^T \tilde{\Gamma}^{-1} \tilde{K}\right) \tag{22}$$

where

$$\begin{aligned} &\tilde{K}(t) \triangleq \left[\tilde{K}_c(t), \tilde{K}_e(t)\right], \tilde{\Gamma} \triangleq \mathrm{blockdiag}(\Gamma_c, \Gamma_e), \\ &\tilde{K}_c \triangleq \hat{K}_c - K_c, \tilde{K}_e \triangleq \hat{K}_e - K_e. \end{aligned} \tag{23}$$

According to (17), the time derivative of (22) with respect to time is presented as (24)assuming that the unknown part in feedback gains are slowly varying, i.e., $\dot{K}_c, \dot{K}_e \approx 0$.

$$\begin{aligned} \dot{V}\left(t, \varepsilon, \hat{K}_c, \hat{K}_e\right) = &-\varepsilon^T Q_t \varepsilon + 2\mathrm{tr}\left(\tilde{K}_c^T \tilde{\Gamma}^{-1} \dot{\hat{K}}_c\right) + 2\mathrm{tr}\left(\tilde{K}_c^T T_{c,n} \varepsilon^T P B\right) \\ &+2\mathrm{tr}\left(\tilde{K}_e^T \tilde{\Gamma}^{-1} \dot{\hat{K}}_e\right) + 2\mathrm{tr}\left(\tilde{K}_e^T e \varepsilon^T P B\right). \end{aligned} \tag{24}$$

Applying the adaptive laws (19) and (20), it holds that

$$\dot{V}\left(t, \varepsilon, \hat{K}_c, \hat{K}_e\right) = -\varepsilon^T Q_t \varepsilon . \tag{25}$$

Since Q_t is chosen to be symmetric and positive-definite, $\dot{V}\left(t, \varepsilon, \hat{K}_c, \hat{K}_e\right)$ is non-positive definite. Therefore, the closed-loop system is uniformly Lyapunov stable and hence, $\varepsilon(t), \hat{K}_c(t), \hat{K}_e(t)$ are uniformly bounded.

Since A is Hurwitz and $r(t)$, namely $T_{cmd}(t)$, is bounded, it follows from (11) and (12) that both $\dot{x}_r(t)$ and $\dot{x}(t)$ are bounded. Since $e_t(t)$ is uniformly bounded, according to (16), $e(t)$ is bounded. Hence, $x(t) = e(t) + x_r(t)$ is bounded. Moreover, since $T_{c,n}$ is bounded, it follows from (18), , and that $u(t)$ is bounded and hence, it follows from (9) and (10) that $\dot{x}(t)$ is bounded. Therefore, $\dot{e}(t) = \dot{x}(t) - \dot{x}_r(t)$ is bounded. Since $\dot{e}_t(t)$ is bounded, $\dot{\varepsilon}(t) = \dot{e}(t) - \dot{e}_t(t)$ is bounded. In addition, $\ddot{V}\left(t, \varepsilon(t), \hat{K}_c(t), \hat{K}_e(t)\right) = -2\varepsilon^T(t)Q_t\dot{\varepsilon}(t)$ is bounded. Consequently, $\dot{V}\left(t, \varepsilon(t), \hat{K}_c(t), \hat{K}_e(t)\right)$ is uniformly continuous according to (Ioannou and Sun, 1995). Hence, it follows from Barbalat's lemma that the closed-loop trajectory tracking error $\varepsilon(t)$ is uniformly convergent to zero.

Moreover, it follows from the triangle inequality that

$$\left\|\varepsilon(t)\right\| \geq \left\|\left\|e(t)\right\| - \left\|e_t(t)\right\|\right\| . \tag{26}$$

Since $e_t(t)$ is uniformly bounded and convergent to zero, $e(t)$ is uniformly bounded and convergent to zero.

3.5 Convergence rate analysis

According to (Boyd, 1994), the convergence rate of $x(\cdot)$ is defined as

$$\alpha_{\max}\left(x(\cdot)\right) \triangleq \sup \liminf_{t \to \infty} \frac{\log\left\|x(t)\right\|}{t_0 - t} . \tag{27}$$

According to (Kågström, 1977), in the classical MRAC, it holds that $\alpha_{\max}\left(e(\cdot)\right) = -\mathrm{Re}\left(\lambda_{\max}(A)\right)$ and there exist $\xi, \gamma_1 \geq 1, \gamma_2 \in (0,1)$ such that

$$\lim_{t\to\infty}\left(\xi(t)-\mathrm{Re}\left(\lambda_{\max}(A)\right)\right)=0^{+}, \tag{28}$$

$$\left\|e(t)\right\|\le\gamma_1\left\|x_0-x_{r,0}\right\|e^{\xi(t)(t-t_0)}-\frac{\gamma_1\|B\|}{\gamma_2\,\mathrm{Re}\left(\lambda_{\max}(A)\right)}\sup_{t\in[t_0,\infty)}\left\|u(t)\right\|. \tag{29}$$

Considering the proposed two-layer MRAC, since $e(t)=\varepsilon(t)+e_t(t)$, there exist $\xi,\gamma_1\ge 1,\gamma_2\in(0,1)$ such that

$$\lim_{t\to\infty}\left(\xi(t)-\mathrm{Re}\left(\lambda_{\max}(A_t)\right)\right)=0^{+}, \tag{30}$$

$$\log\left(\left\|e(t)\right\|\right)\le\log\left(\gamma_1\left\|x_0-x_{r,0}\right\|\right)+\xi(t)(t-t_0)+\log\left(\begin{array}{l}1-\dfrac{\gamma_1\|B\|}{\gamma_2\,\mathrm{Re}\left(\lambda_{\max}(A_t)\right)}\\ \cdot\sup\limits_{t\in[t_0,\infty)}\left\|\begin{array}{l}\hat{K}_c T_{c,n}(t)\\ +\hat{K}_e\left(\varepsilon(t)+e_t(t)\right)\end{array}\right\|\\ \cdot\left[e^{\xi(t)(t-t_0)}\gamma_1\left\|x_0-x_{r,0}\right\|\right]^{-1}\end{array}\right). \tag{31}$$

Therefore, since $\lim_{t\to\infty}\dfrac{\log\left(1-ke^{\lambda(t-t_0)}\right)}{t_0-t}=0$ for all $k>0,\lambda<0$, and $\lim_{t\to\infty}\xi(t)=\mathrm{Re}\left(\lambda_{\max}(A_t)\right)$, it follows from (31) that $\alpha_{\max}\left(e(\cdot)\right)\ge-\mathrm{Re}\left(\lambda_{\max}(A_t)\right)$. In addition, as $\mathrm{Re}\left(\lambda_{\max}(A_t)\right)<\mathrm{Re}\left(\lambda_{\min}(A)\right)$, the convergence rate of the tracking error satisfies the condition that $\alpha_{\max}\left(e(\cdot)\right)\ge-\mathrm{Re}\left(\lambda_{\max}(A_t)\right)>-\mathrm{Re}\left(\lambda_{\min}(A)\right)\ge-\mathrm{Re}\left(\lambda_{\max}(A)\right)>0$.

4. RESULTS AND DISCUSSION

In this section, simulations using MATLAB/Simulink are carried out. focusing on the ESS issue, the transient performance of the proposed two-layer MRAC against uncertain clutch slipping torque and measurement noise is compared to that of the classical MRAC under the driving scenario that the driver demand torque abruptly changes. The faster convergence rate of the proposed method as stated in Section 3.4 is demonstrated.

The vehicle jerk represents the riding comfort of the ESS (Huang and Wang, 2004). It is defined as the derivative of the vehicle acceleration. The mathematical expression is written as

$$jerk=\frac{\mathrm{d}a}{\mathrm{d}t}=\frac{\mathrm{d}^2v}{\mathrm{d}t^2}=R\frac{\mathrm{d}(T_s-T_r/J_v)}{\mathrm{d}t}. \tag{32}$$

It is noted that when the driver pushes the accelerator pedal, there is an expected jerk which represents the output power to the wheels increases, therefore the vehicle acceleration becomes higher. If there is no expected jerk after the accelerator pedal is deepened, the driver may render that the pedal is not deep enough and continue to push the pedal, which can result in safety incidents.

With the reference model described in (11), the control input T_{tm} is given by classical MRAC (Ioannou and Sun, 1995) as

$$T_{tm}(t)=T_{cmd}(t)+T_{c,n}(t)+\hat{K}_{c,c}T_{c,n}(t) \tag{33}$$

where

$$\dot{\hat{K}}_{c,c}(t)=-\Gamma_{c,c}T_{c,n}(t)e^{T}(t)P_cB \tag{34}$$

$$0=A^{T}P_c+P_cA+Q_c \tag{35}$$

and P_c,Q_c are symmetric and positive-definite.

The values of adaptive gain selected for the proposed two-layer MRAC and the classical MRAC are shown in Table I. Much larger adaptive gains can be adopted for the modified control laws of two-layer MRAC compared to those of the classical MRAC to show the enhancement of transient performance.

Table I Assigned uncertainty and measurement noise for simulations

Two-layer MRAC		Classical MRAC
Γ_c	Γ_e	$\Gamma_{c,c}$
50	50	0.1

In the simulations, the ESS starts at 2.80 s, and the driver demand torque is assumed to increase gradually from 100 Nm to 150 Nm at 3.20 s which is just during ESS as seen in Fig. 5 (i)-(ii).A. The assigned uncertainty in the friction coefficient of the clutch is -30 %. In addition, the motor speed ω_{tm} and vehicle speed are corrupted by measurement noise, namely a Gaussian white noise characterized by a frequency of 100 Hz and range of ±1 rad/s.

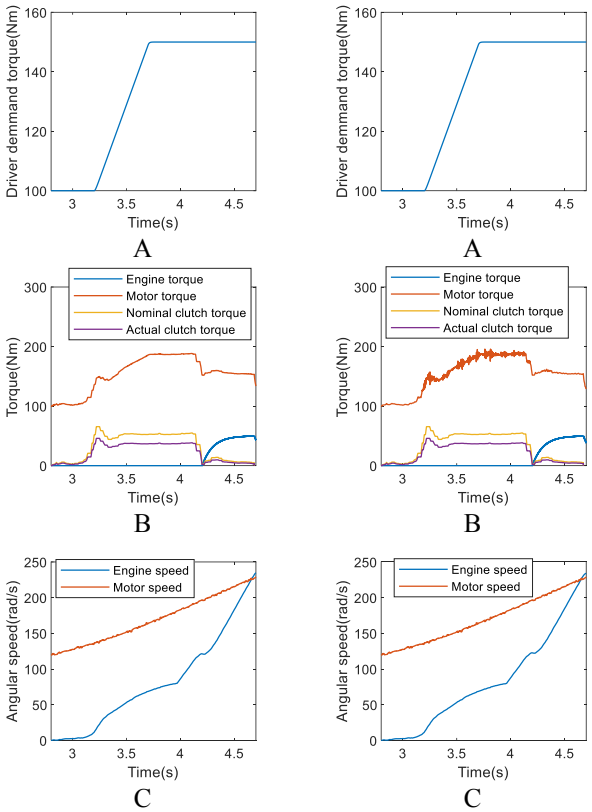

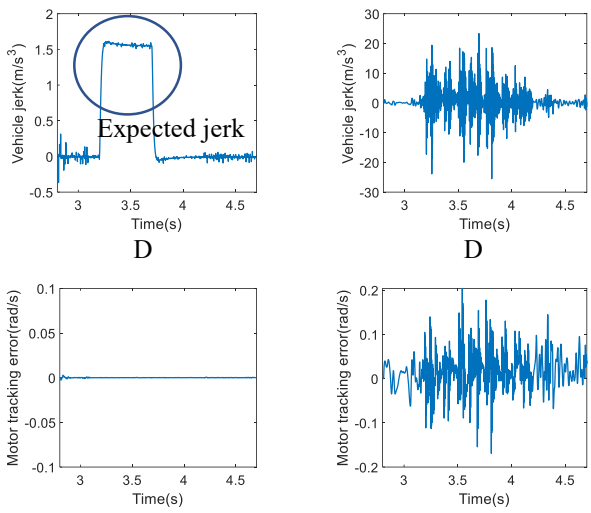

(i) Two-layer MRAC ($\Gamma_c = 50,\ \Gamma_e = 50$)

(ii) Classical MRAC ($\Gamma_{c,c} = 0.1$)

Fig. 5 Comparison between the proposed two-layer MRAC and classical MRAC.

As seen in Fig. 5 (i)-(ii).B, the value of actual clutch slipping torque is smaller than that of the nominal one. As seen in Fig. 5 (i)-(ii).C, guided by the reference profiles generated according to real-time driver demand torque online, both the proposed two-layer MRAC and classical MRAC can respond rapidly to the real-time driver demand torque at 3.20 s.

As stated in Section 3.4, the convergence rate of the two-layer MRAC is higher than that of the classical MRAC. As seen in Fig. 5 (i).E, with the two-layer MRAC, the motor speed shows good tracking performance to the major reference profiles and the tracking error converges to zero quickly against the uncertainty and noise. Meanwhile, there is no obvious fluctuation in motor torque as seen in Fig. 5 (i).B. Therefore, there is no obvious vehicle jerk according to (32), except the expected jerk which is caused by the changes in driver demand torque during 3.20-3.75 s. The results show that the compensation for clutch slipping torque is rapid and accurate. The transient performance of the two-layer MRAC is hence validated. In contrast, there are high-frequency fluctuations in motor torque with classical MRAC, resulting in obvious jerk over 20 m/s^3 during the whole ESS process. Even though the classical MRAC system is stable, the transient performance deteriorates and the riding comfort is unsatisfactory.

5. CONCLUSIONS

In this paper, a novel two-layer MRAC based on state feedback is proposed for the ESS which can satisfy the driver's demand torque and show good transient performance despite the parametric uncertainty in clutch and measurement noise. An auxiliary reference model is introduced to the MRAC system in addition to the major reference model to modify the convergence rate without changing the reference profiles, which is generated according to the real-time driver demand torque. The enhancement on the transient performance of the proposed two-layer MRAC is validated by the comparison to the classical MRAC with large adaptive gains. Considering the shaft torque, which is one of the state variables, cannot be measured directly in production vehicles, the controller is required to be modified in the future work.

References

Anderson, R. B., Marshall, J. A. & L Afflitto, A. (2021), "Novel model reference adaptive control laws for improved transient dynamics and guaranteed saturation constraints", *Journal of the Franklin Institute,* Vol. 358 No. 12, pp. 6281-6308.

Biswas, A., Anselma, P. G., Rathore, A. & Emadi, A. (2021), "Effect of coordinated control on real-time optimal mode selection for multi-mode hybrid electric powertrain", *Applied Energy,* Vol. 289116695.

Boyd, S. P. (1994), Linear matrix inequalities in system and control theory, Philadelphia, Society for Industrial and Applied Mathematics.

Chen, L., Xi, G. & Sun, J. (2012), "Torque Coordination Control During Mode Transition for a Series – Parallel Hybrid Electric Vehicle", *IEEE Transactions on Vehicular Technology,* Vol. 61 No. 7, pp. 2936-2949.

Cong, L., Xing, X., Feng, W. & Zhiguang, Z. (2021), "Coordinated control strategy for mode transition of DM-PHEV based on MLD", *Nonlinear dynamics,* Vol. 103 No. 1, pp. 809-832.

Du, B., Yin, X. & Yang, Y. (2017), "Robust control of mode transition for a single-motor full hybrid electric vehicle", *Advances in Mechanical Engineering,* Vol. 9 No. 9, pp. 168781401771742.

Huang, Q. & Wang, H. (2004), "Fundamental Study of Jerk: Evaluation of Shift Quality and Ride Comfort", *Sae Technical Papers,* Vol. 01.

Ioannou, P. A. & Sun, J. (1995), Robust Adaptive Control, Prentice-Hall, Inc.

Kågström, B. (1977), "Bounds and perturbation bounds for the matrix exponential", *BIT Numerical Mathematics,* Vol. 17 No. 1, pp. 39-57.

Kim, S. & Choi, S. B. (2020), "Cooperative Control of Drive Motor and Clutch for Gear Shift of Hybrid Electric Vehicles With Dual-Clutch Transmission", *IEEE/ASME Transactions on Mechatronics,* Vol. 25 No. 3, pp. 1578-1588.

Peng, C., Chen, L. & Sun, J. (2018), "Model Reference Adaptive Control during Mode Transition of a Parallel Hybrid Electric Vehicle", inAACC, pp. 92-97.

Yang, C., Shi, Y., Li, L. & Wang, X. (2020), "Efficient Mode Transition Control for Parallel Hybrid Electric Vehicle With Adaptive Dual-Loop Control Framework", *IEEE Transactions on Vehicular Technology,* Vol. 69 No. 2, pp. 1519-1532.

Zhang, H., Zhang, Y. & Yin, C. (2016), "Hardware-in-the-Loop Simulation of Robust Mode Transition Control for a Series-Parallel Hybrid Electric Vehicle", *IEEE Transactions on Vehicular Technology,* Vol. 65 No. 3, pp. 1059-1069.

Zhou, S., Walker, P., Tian, Y. & Zhang, N. (2020), "Mode switching analysis and control for a parallel hydraulic hybrid vehicle", *Vehicle system dynamics,* 1-21.